Adsorption of biopolymers onto nanocelluloses for the fabrication of hollow microcapsules

Salvatore Lombardo, Bernard Cathala, Ana Villares

Nanotechnology

Salvatore Lombardo, Bernard Cathala and Ana Villares*

Adsorption of biopolymers onto nanocelluloses for the fabrication of hollow microcapsules

https://doi.org/10.1515/npprj-2021-0040
Received June 7, 2021; accepted August 6, 2021

Abstract: In this work, we studied the multilayer adsorption of cellulose nanocrystals and cellulose nanofibers with other polysaccharides such as xyloglucan and chitosan. We showed that the specific interactions between these biopolymers can be exploited to prepare three-dimensional functional materials. Quartz crystal microbalance studies showed that both biopolymers were adsorbed irreversibly on the nanocellulose surfaces. In aqueous media, the maximum amount of adsorbed polymer was higher for the smaller and more crystalline cellulose nanocrystals, compared to cellulose nanofibers. For both nanocelluloses employed, the amount of xyloglucan of the first bilayer was larger than the amount of chitosan adsorbed. Ellipsometry showed that both xyloglucan and chitosan were adsorbed on nanocellulose surfaces. However, at the second layer no mass change was detected by quartz crystal microbalance when xyloglucan was added, while for addition of successive layers of chitosan a decrease of frequency was detected. The water uptake of multilayers was higher for cellulose nanocrystals than for nanofibers, which was ascribed the presence of voids in the nanocrystal layer. Finally, we demonstrated that multilayer adsorption of these biopolymers can be performed on calcium carbonate sacrificial templates, which can then be removed to yield hollow polysaccharide microcapsules.

Keywords: adsorption; chitosan; microcapsule; nanocellulose; xyloglucan.

Introduction

Over the last two decades, there has been significant development in the area of nanocelluloses and their applications (Eichhorn et al. 2011, Klemm et al. 2018). There are two main types of nanocelluloses: cellulose nanofibers (CNF) and cellulose nanocrystals (CNC). CNF are obtained by mechanical delamination of the cellulose fiber, and consist of alternating crystalline and amorphous regions, which are around 5–20 nm in width and several microns in length. CNC are obtained by acid hydrolysis, resulting in crystalline, rigid, rod-like crystallites whose dimensions are around 5–20 nm in width and 200–1000 nm in length, depending on their biological origin (Lin et al. 2012, Moreau et al. 2016). Both CNF and CNC are widely used in applications including gels/foams, thickeners/stabilizers as well as reinforcing agents. The properties of nanocelluloses have triggered much research and innovation on the topic during the last two decades evidencing the new potential for groundbreaking innovations in different areas including food and composites, cosmetics, wound dressings, medical implants, and tissue engineering and drug carriers (Charreau et al. 2020).

An important challenge in the development of nanocelluloses as a novel source of sustainable building blocks for the design of materials remains in their ability to adapt their properties to industrial applications. By carefully controlling interactions with the surrounding material and the hierarchical structure that is formed as a result, we may be able to engineer materials with an unprecedented variety of mechanical properties as well as new functionalities. One strategy for surface modification is the adsorption of polymers on the nanocellulose surface. Early studies have demonstrated that it is possible to use nanocelluloses to form self-assembled layer-by-layer architectures together with oppositely charged polyelectrolytes or nanoparticles or by combining anionic and cationic nanocelluloses directly (Wagberg and Erlandsson 2020).

In this work, we combined the two available nanocelluloses, CNF and CNC, with two common polysaccharides, xyloglucan (XG) and chitosan (Chit), to fabricate multilayer structures on different templates. Layer-by-layer structures were deposited onto sacrificial templates to fabricate hollow stable microcapsules. Nanocellulose microcapsules have attracted much attention, and has been focus of recent reviews (Dias et al. 2015, Corrêa-Filho et al. 2019, Lombardo and Villares 2020). Nanocelluloses could

***Corresponding author: Ana Villares,** INRAE, UR BIA, F-44316, Nantes, France, e-mail: ana.villares@inrae.fr, ORCID: https://orcid.org/0000-0001-5441-7299
Salvatore Lombardo, Bernard Cathala, INRAE, UR BIA, F-44316, Nantes, France, e-mails: salvatore.lombardo@inrae.fr, bernard.cathala@inrae.fr

be used in a biomimetic approach to prepare microcontainers inspired by Nature. Both CNF and CNC have been combined with other polysaccharides to fabricate hollow capsules. Hence, Paulraj et al. (Paulraj et al. 2017, Paulraj et al. 2018a, Paulraj et al. 2018b, Paulraj et al. 2020) have prepared CNF-based capsules on sacrificial $CaCO_3$ templates by combination with plant cell wall polysaccharides including pectins and xyloglucan. However, in all cases, CNF were functionalized with cationic quaternary ammonium groups, in an attempt to favor the interaction with negatively charged pectins. On the other hand, CNC have been assembled with alginate (Lin et al. 2011, Huq et al. 2012) or chitosan (Mohanta et al. 2014) for tuning the swelling behavior of microcapsules. Indeed, CNC acted as an ionic cross-linking agent and filler for the matrix, which decreased porosity and tuned permeability.

Nanocellulose-loaded microcapsules would represent a promising platform for the development of novel drug-delivery systems and other biomedical applications, such as biosensors. In this work, we studied layer-by-layer deposition of cellulose nanomaterials of varying length (CNC and CNF) functionalized with carboxylic acid groups, which have not been used before to prepare multilayer films and microcapsules in combination with other biopolymers. Also, the effect of grafting of a fluorophore was studied. Our work demonstrate that the interactions between different natural polysaccharides can be used for the preparation of supramolecular architectures, such as films and hollow microcapsules.

Materials and methods

Materials

TEMPO-oxidized cellulose nanofibers (CNF) were purchased from EMPA Materials Science and Technology (Switzerland). The charge density was 1.1 mmol g^{-1}, as previously reported (Jiménez-Saelices et al. 2017). Cellulose nanocrystals (CNC) were purchased from the University of Maine Process Development Center (United States). CNF and CNC were dispersed at 1 g L^{-1} in deionized water (18.2 MΩ, Millipore Milli-Q purification system). Xyloglucan (XG) from *Tamarindus indica* was provided by DSP Gokyo Food & Chemical (Japan). Aqueous XG solutions (2 g L^{-1}) were prepared with deionized water. Chitosan (Chit) was purchased from Sigma Aldrich (degree of deatecylation was 75–85 %, Brookfield viscosity 20000 cps). Aqueous chitosan solutions (2 g L^{-1}) were prepared by adding few drops of 1 M hydrochloric acid until pH was lower than 3. Commercial $CaCO_3$ microspheres (Mikhart) were supplied by Provençale S. A. Poly(allylamine hydrochloride) was purchased from Polysciences Inc. 2,2,6,6-Tetramethylpiperidine 1-oxyl radical (TEMPO), fluorescein isothiocianate, rhodamine B isothiocyanate, dibutyltin dilaurate, pyridine, hydrochloric acid, sodium hypochlorite, potassium bromide, sodium carbonate, calcium chloride, methanol, and dimethyl sulfoxide were purchased from Sigma Aldrich.

Synthesis of TEMPO-oxidized cellulose nanocrystals

TEMPO-mediated surface oxidation of cellulose nanocrystals was performed as previously reported (Habibi et al. 2006). 2 g of CNCs suspension were diluted to ≈ 200 mL, and the mixture was dispersed by sonication (30 s, 50 % amp). 1.2 g of NaBr were added to the resulting suspension. Then, 5 mL of NaClO and 120 g of TEMPO were added to the suspension under stirring. The pH was maintained at 10 with a NaOH solution freshly prepared. To maintain the pH an automatic program was used with an autotitrator (TIM900 titration manager). The reaction was continued for 45 minutes, until the pH change was low. The reaction was quenched adding 10 mL of methanol. Then, the suspension was dialyzed (MWCO 12–14000 g mol^{-1}) with Milli-Q water for 15 days. The surface charge was 1.1 mmol g^{-1}.

Fluorescence labeling of polysaccharides

CNC and CNF were labelled with a fluorophore (either fluorescein or rhodamine) as previously described (Belder and Granath 1973). Briefly, 1 g of polysaccharides was dispersed in 40 mL of DMSO. Either 10 mg of fluorescein isothiocyanate or 7.5 mg of rhodamine B isothiocyanate were added to the solution. Then, 50 µL of dibutyltin dilaurate and after few drops of pyridine were added to the suspension. The reaction mixture was left to stir at 65 °C for 2 h under dark. The reaction mixture was filtered using vacuum filtration (funnel with pore n. 3). CNF were thoroughly washed with ethanol until the filtrate was clear. CNC were washed with 1 M NaCl. The polysaccharide suspensions were dialyzed (MWCO 12–14000 g mol^{-1}) with Milli-Q water for 15 days.

Preparation of $CaCO_3$ sacrificial template (microparticles)

$CaCO_3$ microparticles were prepared according to Paulraj et al. (Paulraj et al. 2017), by mixing with 1 M $CaCl_2$ and 1 M

Na_2CO_3 together under mechanical stirring for 60 s, and incubated for 30 min. After incubation, the particles were washed with water by centrifugation 6 times (5000 rpm, 60 s), and dried at 80 °C for 2 h. Particles were stored at RT in closed containers. As comparison, commercial $CaCO_3$ microspheres, which had a smaller average diameter, were also used. A comparison of the $CaCO_3$ microspheres used is shown in the supporting information (Figure S1).

Nanocellulose microcapsule preparation

The nanocellulose-coated microcapsules were prepared by dispersing 25 mg of $CaCO_3$ microparticles in 100 mM NaCl (10 mL) and sonicated (30 s with 50 % amplitude). Then, the $CaCO_3$ microparticles suspension was incubated with 1 mg of CNF or CNC suspension in 100 mM NaCl for 15–30 min under constant mixing, followed by washing thrice with 100 mM NaCl. Subsequently, 2 mg of XG or Chit (in 100 mM NaCl) were added, and incubated for at least 15 min followed by washing thrice with 100 mM NaCl. The cycle was repeated until five bilayers were obtained. The pH of the suspension was around 9, as expected for a supersaturated solution of $CaCO_3$. In order to obtain the hollow microcapsules, the particles were treated with HCl 1 M until the pH of the solution was lower than 3. After the treatment, the microcapsules were washed thrice with water by centrifugation. For comparative studies and to understand the effect of NaCl, microcapsules were also produced with the same procedure using polysaccharides dispersed in Milli-Q water (Paulraj et al. 2017).

Conductometry

The surface charge of CNF and CNC was measured by conductometric titration with a 0.015 M NaOH solution by a TIM900 titration manager and a CDM230 conductometer equipped with a CDC749 conductivity cell. The surface charge (mmol g^{-1}) was determined by the following equation (Habibi et al. 2006):

$$Surface\ charge = \frac{162 C_{NaOH} V_{NaOH}}{m - 36 C_{NaOH} V_{NaOH}} \quad (1)$$

Where C_{NaOH} is the NaOH concentration (mol L^{-1}), and V_{NaOH} is the volume of NaOH (L), m is the dried mass of cellulose (g); 162 is the molecular weight of the anhydroglucose unit; and 36 corresponds to the difference between the molecular weight of an AGU and that of the sodium salt of the TEMPO-oxidized anhydroglucose unit.

Quartz crystal microbalance with dissipation (QCM-D) experiments

QCM-D experiments were carried out with a Q-Sense E4 instrument (AB, Sweden) using a piezoelectric AT-cut quartz crystal coated with gold electrodes on each side (QSX301, Q-Sense). Frequency ($\Delta f_n/n$) and (ΔD_n) dissipation changes were simultaneously registered at 5 MHz fundamental resonance frequency and its several overtones as a function of time. The third overtone (15 MHz) was used in the evaluation of the QCM-D data. The surface concentration (Γ) can be deduced from the frequency change ($\Delta f_n/n$) by using the Sauerbrey's equation (Sauerbrey 1959):

$$\Gamma = -C\frac{\Delta f_n}{n} \quad (2)$$

where C is the constant for the mass sensitivity of the quartz crystal (0.177 mg m^{-2} Hz^{-1} for 5 MHz crystal), and n is the overtone number.

Gold-coated quartz crystals were cleaned in piranha solution H_2SO_4/H_2O_2 (7:3, v/v), rinsed exhaustively with Milli-Q water, and dried under a stream of nitrogen. Prior to use, QCM-D quartz sensors were subjected to a plasma etching device (Harrick Plasma).

Adsorption of biopolymers

A baseline was first established by continuously flowing pure water solution on the quartz crystal surface, then frequency and dissipation signals were off-set to zero just before injection of polymer solutions in a continuous mode at a flow rate of 0.1 mL min^{-1}. CNF or CNC dispersions (at 0.1 g L^{-1}) and XG or Chit solutions (at 0.2 g L^{-1}) were alternately injected into the QCM-D cell until a plateau value of frequency and dissipation signals was reached. Then, a rinsing step of the surface with pure water was performed before the subsequent injection of polymer solution. QCM-D experiments were carried out twice.

Determination of water content (or solvent fraction)

CNF/XG/CNF, CNF/Chit/CNF, CNC/XG/CNC and CNC/Chit/CNC films were previously deposited onto the quartz crystal substrates. CNF or CNC dispersions (1 g L^{-1}) were dropped on a pre-coated substrate with poly(allylamine hydrochloride) (PAH) at 2 g L^{-1} in water and, after 10 min of adsorption, excess of polymers was removed,

rinsed with Milli-Q water, and dried under a stream of nitrogen. Then, XG or Chit solutions (2 g L^{-1}) were dropped on the substrate, allowed to adsorb for 10 min, removed the excess of polymers, rinsed with Milli-Q water, and dried under a stream of nitrogen. The next layer of CNF or CNC was adsorbed using the same conditions.

The water mass, Γ_{water}, associated to the nanocrystal layers was estimated by the H_2O/D_2O solvent exchange procedure monitored by QCM-D (Kittle et al. 2011, Kittle et al. 2012). Films were first allowed to swell in water for 2 h at a flow rate of 100 µL min^{-1} until the resonance signal was stable. Then, frequency and dissipation signals were offset to zero and deuterated water was introduced into the flow cell at a rate of 100 µL min^{-1}. After 10 min, water was again injected into the cell and the frequency returned to the initial baseline. From the differences in the frequency changes between the bare quartz crystals $(\Delta f_n/n)_{bare}$ and the films $(\Delta f_n/n)_{film}$, the drop in frequency due to the water content $(\Delta f_n/n)_{water}$ can be calculated according to the following expression (Kittle et al. 2011):

$$\left(\frac{\Delta f}{n}\right)_{water} = \frac{\left(\frac{\Delta f_n}{n}\right)_{film} - \left(\frac{\Delta f_n}{n}\right)_{bare}}{\left(\frac{\rho_{D_2O}}{\rho_{H_2O}}\right) - 1} \quad (3)$$

where $(\Delta f_n/n)_{film}$ and $(\Delta f_n/n)_{bare}$ are the frequency changes observed when D_2O is introduced into the cell for the film and the bare quartz substrate, respectively, n the overtone number, and ρ_{D_2O} and ρ_{H_2O} the densities of deuterated and hydrogenated water, respectively. The water surface concentration, Γ_{H_2O}, is then calculated from $(\Delta f_n/n)_{water}$ using the Sauerbrey's equation (Equation 2).

Ellipsometry

Silicon wafers were cleaned in piranha solution H_2SO_4/H_2O_2 (7:3, v/v), rinsed exhaustively with Milli-Q water, and dried under a stream of nitrogen. CNF/XG/CNF, CNF/Chit/CNF, CNC/XG/CNC and CNC/Chit/CNC films were prepared as described above.

Film thickness was measured using a variable-angle spectroscopic ellipsometer (M-2000U; J. A. Woollam, Lincoln, USA). The ellipsometric angles, Δ and Ψ, were acquired over the spectroscopic range 250–1000 nm at three angles of incidence 65, 70 and 75°. Average thickness values were obtained from the measurement of at least 6 spots per film. Optical modeling and data analysis were performed using the CompleteEASE software package (J. A. Woollam Co., Inc.) using a three-layer model consisting on the Si(100) substrate, a thin SiO_2 layer, and the single Cauchy layer describing the nanocellulose layer and taking into account the surface roughness (~ 5 nm).

ξ-potential

ξ-potential experiments were performed with a Malvern NanoZS instrument. All measurements were made at a temperature of 20 °C with a detection angle of 12.8°. CNF and CNC dispersions were diluted to 0.1 g L^{-1} and XG and Chit solutions at 0.2 g L^{-1} and filtered by 5 µm.

Confocal microscopy

Capsules of labelled polysaccharides were imaged by confocal microscopy (Leica TCS-SP2). Confocal images of the microcapsules were acquired with LSM-510 UV–vis equipped with 63 × 1.2 water immersion objectives (Zeiss, Germany). The microcapsule's structural morphology was studied by adding rhodamine 6G and FITC. Excitation/emission wavelengths were 530/566 for rhodamine and 488/515 nm for fluorescein.

Results and discussion

QCM-D study of the adsorption of biopolymers

The adsorption of biopolymers was monitored by quartz crystal microbalance with dissipation monitoring (QCM-D). Firstly, a stable baseline was established prior to adsorption of biopolymers. QCM-D substrates were precoated with a poly(allylamine hydrochloride) (PAH) layer. Then, biopolymers were sequentially injected onto the quartz crystal surface in a continuous flow until a steady-state signal of frequency (Δf) and dissipation (ΔD) was reached, allowing polymer adsorption to reach equilibrium. A rinsing step, with Milli-Q water, was included between cellulose and xyloglucan or chitosan adsorption stages, in order to remove all polymers that were loosely bound to the surface. Figure 1 shows the evolution of normalized frequency ($\Delta f_n/n$) and dissipation ($\Delta D_n/n$) signals for overtone number $n = 3$ as a function of time for CNF and CNC dispersions at 0.1 g L^{-1} and for XG and Chit solution at 0.2 g L^{-1}.

The decrease of frequency signal ($\Delta f_n/n$) after each polymer injection, concomitantly with an increase of dissipation signal, evidenced that hydrated mass (polymer with coupled water) was being adsorbed at the gold sur-

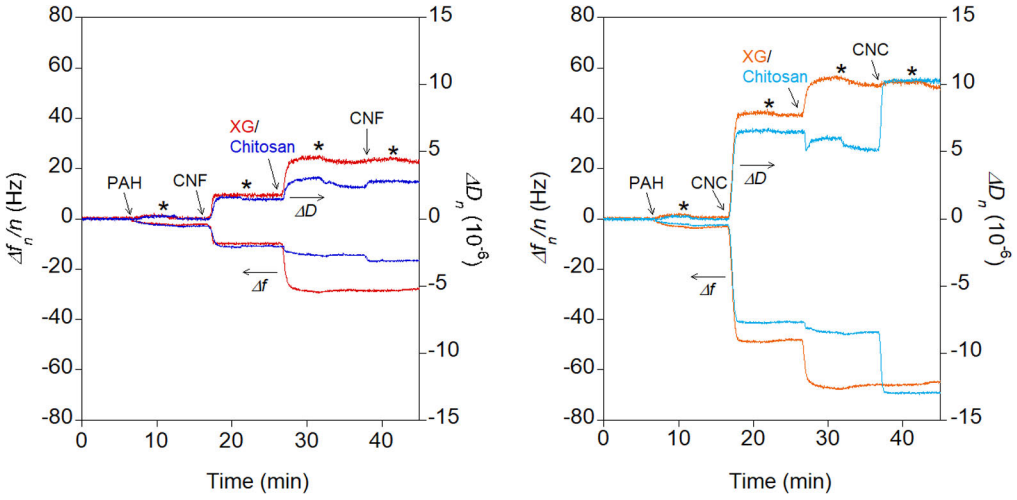

Figure 1: Frequency ($\Delta f_n/n$) and dissipation ($\Delta D_n/n$) changes for the overtone number $n = 3$ during adsorption of CNF (left panel) and CNC (right panel) dispersions at 0.1 g L^{-1} and XG or Chit solutions (0.2 g L^{-1}) on the gold surface of the QCM-D sensor as function of time. Arrows indicate the injection of the polymers and the asterisks indicate the rinse steps with water in between.

face. Complete adsorption was assessed when the plateau of frequency and dissipation signals was reached. Upon rinsing, no significant change in frequency was observed, which indicated the irreversible adsorption of biopolymers at the studied conditions. When Chit was adsorbed on CNC layers, dissipation and frequency decreased simultaneously. Considering that CNC and CNF have a comparable surface charge, we can associate this effect to dewatering occurring when Chit was adsorbed on CNC. This showed that the binding was entropy driven, in agreement with previous findings, which proved that the adsorption of charged molecules on nanocellulose surface is driven by the increase of entropy associated to the release of water molecules from the nanocellulose surface (Lombardo and Thielemans 2019).

The injection of CNF resulted in a lower frequency decrease and dissipation increase than the injection of CNC. Previous studies have shown that the adsorption of negatively charged CNF generally involves a frequency decrease between –20 and –50 Hz (Ahola et al. 2008a, Aulin et al. 2010, de Castro et al. 2018), depending on adsorption conditions and the CNF nature whereas the adsorption of CNC may attain frequency changes of –100 Hz (Olszewska et al. 2013). This difference can be linked to the fact that cellulose nanocrystals have a higher number of binding sites compared to nanofibers, which could be associated to the higher surface area and crystallinity of smaller and more rigid rod-shaped nanocrystals. Interactions between nanocellulose and xyloglucan are highly specific, and the main driving force is linked to hydrogen bonds and van der Waals interactions (Zhang et al. 2011).

Concerning the adsorption of soluble polysaccharides onto cellulose, the adsorption of XG on both CNF and CNC resulted in greater frequency and dissipation changes compared to Chit, as previously described for their adsorption onto neutral CNF (Eronen et al. 2011). The subsequent injection of CNF or CNC resulted in lower changes in frequency and dissipation in the case of Chit, and no noticeable changes in the case of xyloglucan. Compared to neutral xyloglucan, the positive charge of Chit could favor the electrostatic interaction and therefore the adsorption of the second layer of CNF and CNC. An example of QCM experiment showing 5 CNC/Chi bilayers adsorption of is shown in the supporting information (Figure S2).

In order to get more insight into the adsorption of biopolymers, we studied the change of dissipation as a function of the frequency ($\Delta D_n - \Delta f_n/n$), as shown in Figure 2.

The $\Delta D_n - \Delta f_n/n$ plots reveal at any point of the curve how dissipation changes by frequency unit allowing a comparison of the viscoelasticity characteristics of the films (Rodahl et al. 1997, Ahola et al. 2008b). Changes in the $\Delta D_n - \Delta f_n/n$ slope revealed different biopolymer arrangements on the surface. Hence, high values of the slope are characteristic of thick, hydrated, and viscoelastic layers whereas a rigid and compact layer would yield a small slope. For the adsorption of the first layer of CNF and CNC, in both cases ΔD_n increased linearly with increasing $\Delta f_n/n$, which suggested that the cellulose nanomaterials did not undergo significant conformational changes in the course of the adsorption process (Amirkhani et al. 2008). The slopes were -0.25 ± 0.02 and -0.17 ± 0.00 Hz^{-1},

Table 1: Surface mass concentration (Γ) calculated by the Sauerbrey's equation by *in situ* ellipsometry in air (dry) and in water (wet) of the films fabricated by layer-by-layer deposition. Results are expressed as mean ± standard deviation.

	CNF/XG/CNF	CNF/Chit/CNF	CNC/XG/CNC	CNC/Chit/CNC
Γ_{dry} (mg m^{-2})	264.8 ± 41.3	195.0 ± 5.8	12.5 ± 1.5	8.8 ± 2.9
Γ_{wet} (mg m^{-2})	371.2 ± 31.9	324.5 ± 21.4	27.5 ± 4.4	47.6 ± 2.9
%H_2O	29 ± 5	40 ± 2	54 ± 2	82 ± 5

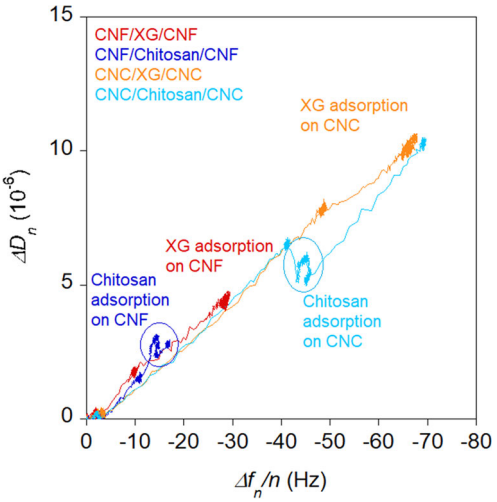

Figure 2: Change of dissipation as a function of the change in frequency ($\Delta D_n - \Delta f_n/n$) for the overtone $n = 3$ corresponding to the successive adsorption of CNF or CNC dispersions (0.1 g L^{-1}) and XG or Chit solutions (0.2 g L^{-1}).

for CNF and CNC, respectively. These values pointed at the nanocellulose adsorption as a rather thin layer on the substrate, which is expected when linear polycations such as PAH are used as a first layer at low ionic strength (Martin and Bruno 2014). Previous work has shown the formation of flat monolayers of few nm for both CNC (Cranston and Gray 2006) and CNF (Wagberg et al. 2008). When XG was adsorbed onto cellulose, a linear behavior was again observed, and the absolute value of the slope decreased to −0.14 Hz^{-1}, indicating the formation of a slightly more rigid layer. The slope of XG adsorption was the same for both CNF and CNC surfaces, which suggested that the arrangement of XG at the surface was not impacted by the presence of crystalline/amorphous regions. Differently, the adsorption of Chit showed an initial linear region followed by a loop. The presence of several slopes during adsorption can be associated with multiple adsorption stages. This fact can be explained by a first interaction between the polysaccharide chains of chitosan and cellulose, which was characterized by the linear change of the slope, and the subsequent conformational change of Chit illustrated by the loop observed in the $\Delta D_n - \Delta f_n/n$ plot. From the linear region, the absolute value of the slope increased to −0.46 ± 0.06 Hz^{-1} and 0.50 ± 0.29 Hz^{-1}, for CNF and CNC, respectively. Note that in the case of CNF, the slope was negative whereas for CNC the slope was positive, which demonstrated that the Chit adsorption can be associated to the concomitant dewatering effect observed upon adsorption of Chit on CNC, and demonstrated that the adsorption behavior was strongly dependent on the structural organization of the layer. Then, the adsorption of the second layer of nanocellulose onto the Chit layer showed a different behavior depending on CNF or CNC. Hence, for CNF, the slope decreased to −0.16 ± 0.01 Hz^{-1} whereas for CNC the slope increased to −0.21 ± 0.01 Hz^{-1}.

Fabrication and properties of the films

The interaction between polysaccharides allowed the fabrication of cellulose-XG/Chit-cellulose assemblies by the layer-by-layer procedure. Dry masses of the films were calculated from the difference in frequency of bare gold substrate and the frequency after the film deposition on the gold substrate. The frequency difference was then converted into mass by means of the Sauerbrey's equation (Equation 2). At the dry state, the CNF films showed higher surface concentration than those containing CNC (Table 1, first line). Comparing XG and Chit, for both CNF and CNC, XG assemblies showed higher surface concentration.

The water uptake of the cellulose films was studied by the H_2O/D_2O solvent exchange procedure monitored by QCM-D. This method allows calculating the solvent fraction of the films by evaluating the differences in their resonant frequency when the solvent changes from H_2O to D_2O (Kittle et al. 2011). Figure 3 shows representative plots of frequency versus time for cellulose films deposited onto a gold substrate, switched from H_2O to D_2O and back to H_2O.

The frequency shift observed upon D_2O injection for CNF films was larger in all cases than the corresponding for the CNC films. Indeed, re-injection of H_2O did not yield initial frequency and dissipation values for the CNF films. This different behavior between CNF and CNC could indi-

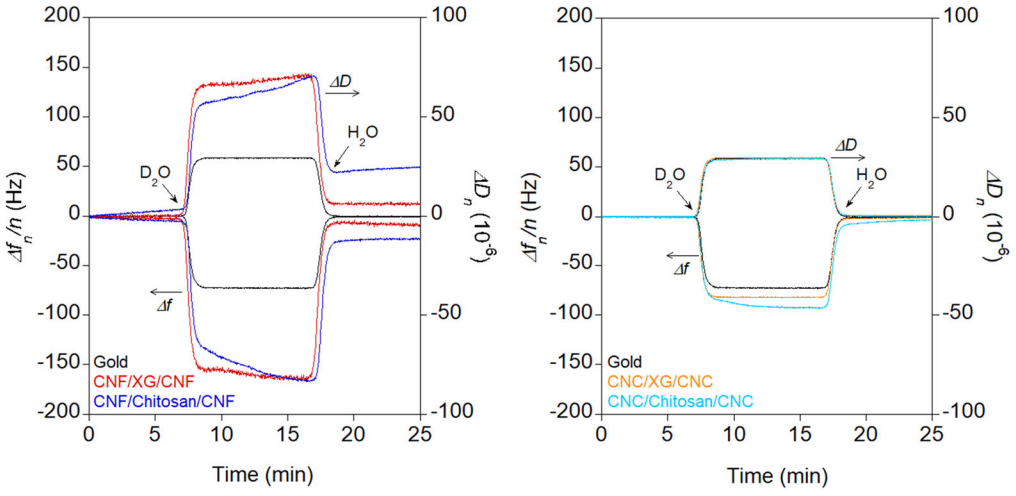

Figure 3: Representative H_2O/D_2O solvent exchange frequency data of a bare gold sensor (black lines) and the CNF and CNC films for the overtone number $n = 3$.

cate that CNF films followed different water uptake process comprising nanofiber arrangements that increased the water content of the CNF film. The percentage of water in the swollen films was calculated by comparing the dry mass and water uptake (Table 1, third line). In all cases, taking into account the dried mass deposited onto the gold substrate, the water content was higher for CNC than for CNF films. Water content of CNF films was consistent with about five water molecules per anhydroglucose unit as previously described for regenerated cellulose surfaces (Kittle et al. 2011). More precisely, CNF/XG/CNF films contained four water molecules per anhydroglucose unit and CNF/Chit/CNF films contained six. The presence of amorphous regions in CNF induced the formation of a more flexible layer, which allowed water to penetrate into the cellulose structure and swell (Hatakeyama and Hatakeyama 1998, Muller et al. 2000). Differently, CNC films contained higher percentage of water, eleven molecules of water per AGU for CNC/XG/CNC and forty for CNC/Chit/CNC. The higher water content of crystalline cellulose has been already described and it has been explained in terms of the porosity of the crystalline layer (Kittle et al. 2011). Even if nanocrystals are hydrated and water forms a 1 nm thick layer enveloping the crystal (Niinivaara et al. 2015), the high water content obtained for the CNC films may arise from the voids between crystals in the CNC layer and the water uptake from the soluble polysaccharide (XG or Chit).

Fabrication of multilayer microcapsules

We took advantage of the interaction between polysaccharides for building-up supramolecular architectures. To prepare layer-by-layer microcapsules, CNF or CNC and XG or Chit were adsorbed on $CaCO_3$ sacrificial templates in NaCl 100 mM. Microcapsules were also prepared in water for comparison, but for CNC the salt was necessary to decrease colloidal stability and avoid losing a large amount of material upon washing. Also, the microcapsules were washed in water for better observation, showing very small differences with the NaCl system, therefore demonstrating that the ionic strength has little effect on microcapsules stability. The charge reversal upon layer deposition was monitored by the values of ξ-potential. Upon the adsorption of nanocelluloses on the $CaCO_3$ surface, the ξ-potential of the mixture was −22.2 ± 0.6 and −20.2 ± 1.0 mV for CNF and CNC, respectively. Then, the adsorption of xyloglucan yielded −8.8 ± 0.7 mV on CNF and −6.72 ± 0.3 mV on CNC. Differently, the adsorption of chitosan shifted the ξ-potential to positive values, yielding 22.1 ± 2.9 mV for CNF and 25.3 ± 3.1 mV for CNC. The ξ-potential change upon each polysaccharide adsorption demonstrated the layer-by-layer adsorption. The colloidal stability was observed in a test tube, and was confirmed by particle size analysis, which showed an increase of particle size when the first bilayer was added, while the average diameter increased only slightly when the other bilayers were added (see Figure S3). It should be emphasized that the particles formed large aggregates, and this resulted in a large size distribution, and to a larger average diameter than what observed by microscopy.

In order to get more insight into the multilayer formation, CNF or CNC and XG or Chit were alternatively deposited onto solid supports by the layer-by-layer method. Ellipsometry was used to determine the increase of the thickness of the film when additional layers are added.

Ellipsometry measures the thickness of a dried film and is complementary to QCM, which measure the hydrated mass. Figure 4 shows the variations in thicknesses measured by ellipsometry.

In the case of CNF films, the thickness showed a linear increase with the number of bilayers. The deposition of CNF resulted in a greater increase than the deposition of xyloglucan or chitosan, which was expected because of the different dimensions, as previously observed for chitin nanocrystals (Villares et al. 2014). In the case of CNC, the growth showed a similar linear behavior up to 3 bilayers and then, the deposition resulted in a lower increase in thickness. Ellipsometry results demonstrated the deposition of more than one bilayer for the nanocellulose/xyloglucan systems.

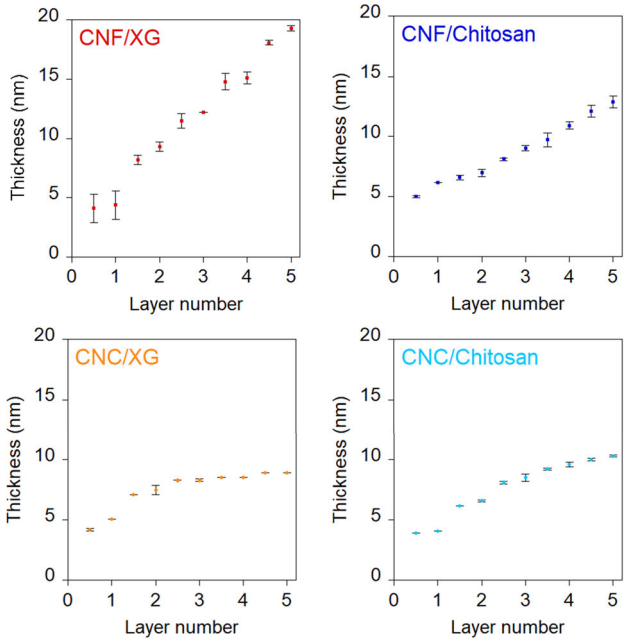

Figure 4: Growth in layer thickness of the CNF and CNC films as a function of the number of layers deposited on a silicon wafer, as measured by ellipsometry. Fractional number indicate CNF or CNC deposition and whole numbers indicate XG or Chit deposition.

We coated $CaCO_3$ capsules by alternating nanocellulose layers and xyloglucan or chitosan using the same protocol as for the film deposition. We labelled CNC and CNF with fluorescence probes, in order to visualize the polysaccharides coating of the capsules. CNF were labelled with rhodamine (red) and CNC were labelled with fluorescein (green). We prepared several batches varying labeling and also without label, in order to see if the fluorophore would have an effect on the interactions between polysaccharides, and therefore on the multilayer adsorption. However, grafting of a fluorescent marker in either nanocellulose or xyloglucan showed no effect on the interactions between components and on the structural stability of the microcapsules. The successful deposition on the sacrificial $CaCO_3$ template was confirmed by optical microscopy and confocal laser scanning microscopy (CLSM). An increase of fluorescence emission was observed under fluorescence microscopy (see Figure S4), which is a further proof of the successful multilayer adsorption. Figure 5 shows the CLSM images of the five-bilayer coated $CaCO_3$ capsules.

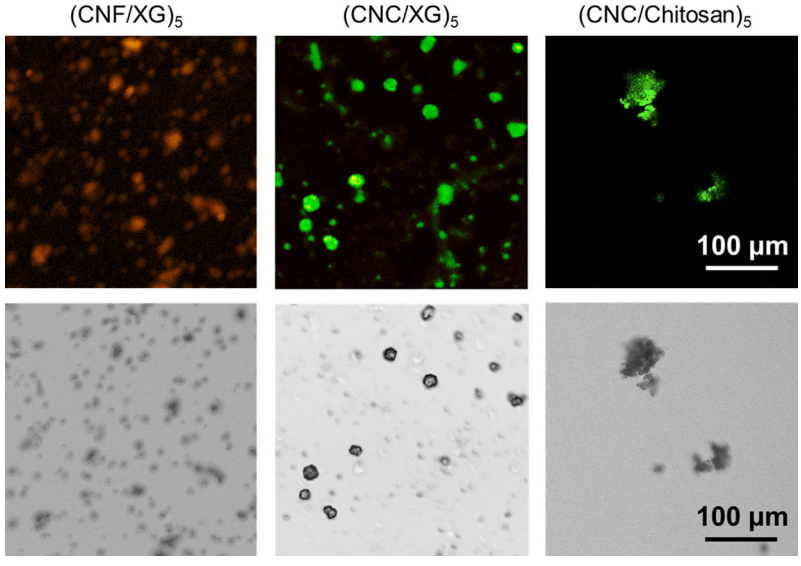

Figure 5: CLSM images (top) and corresponding transmission light microscope images (bottom) of $CaCO_3$ capsules coated with $(CNF/XG)_5$, $(CNC/XG)_5$ and $(CNC/Chit)_5$.

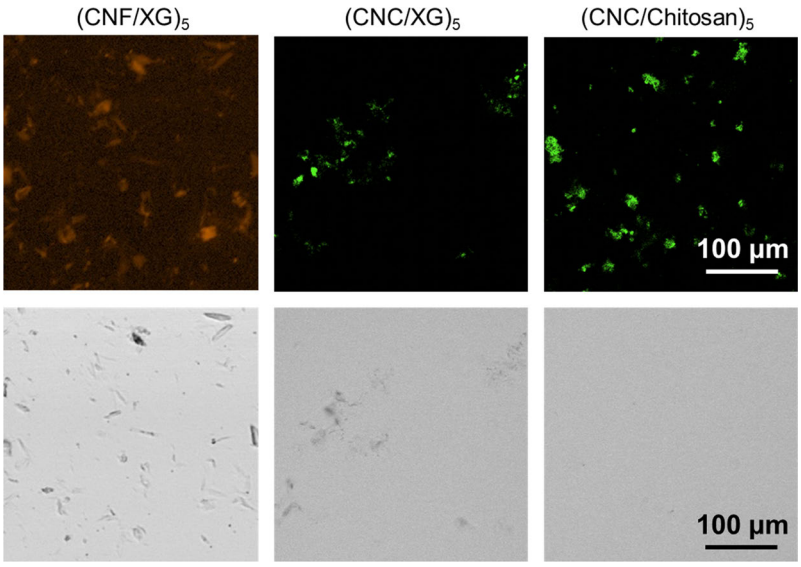

Figure 6: CLSM images (top) and corresponding transmission light microscope images (bottom) of $CaCO_3$ capsules coated with $(CNF/XG)_5$, $(CNC/XG)_5$ and $(CNC/Chit)_5$ after core removal by acid treatment.

When the $CaCO_3$ capsules were coated with XG, for both CNF and CNC we observed individual particles, whereas when the coating contained Chit, capsules aggregated and formed clusters. Paulraj et al. have previously observed that cationic CNF/XG microcapsules aggregate after the deposition of 5 bilayers on $CaCO_3$ (Paulraj et al. 2018a). The sacrificial $CaCO_3$ templates of the layer-by-layer assemblies were removed by acid treatment, adding 1 M HCl dropwise until pH was lower than 2, which solubilized $CaCO_3$. To further confirm that the core removal was complete, the addition of HCl was followed in an optical microscope (see Figure S5). The calcium ions were then removed by washing with Milli-Q water. In their work, Paulraj et al. observed that core removal resulted in significant aggregation between the coated cationic CNF/XG capsules. In our study, we used TEMPO-oxidized CNF and CNC; therefore, the release Ca^{2+} ions could stabilize the microcapsule wall by cross-linking the carboxylic acid groups from the TEMPO oxidation (Lombardo et al. 2019). Thus, complete core removal resulted in hollow microcapsule structures that were structurally stable (Figure 6).

The transmission light microscopy image clearly showed the core removal. The size and shape of the obtained hollow microcapsules correlated well with that of the starting $CaCO_3$ particles coated with CNC. When coated with CNF the particles lost the spherical shape, and this was associated to the higher flexibility of CNF, which could promote the formation of interconnecting networks, thus creating larger aggregates. Template entanglement by CNF has been already described for the stabilization of oil droplets in water (Jiménez-Saelices et al. 2018). Differently from CNC, which form stable monolayers that cover the whole oil droplet (Kalashnikova et al. 2013, Cherhal et al. 2016), CNF form aggregates of interconnected small droplets. The authors ascribed the cross-linking behavior to the high CNF length compared to the droplet diameter and to the higher flexibility imparted by the less ordered domains that induce a gel-like network of droplets. This resulted in less stable systems, as previously described by Paulraj et al. for the microcapsules coated with cationic CNF, pectin and xyloglucan multilayer structures (Paulraj et al. 2018a). For this reason, we prepared capsules with Chit only using CNC as nanocellulose component. As observed before core removal, $(CNF/XG)_5$ and $(CNC/XG)_5$ capsules were individual whereas $(CNC/Chit)_5$ capsules formed some clusters. In the case of XG, for both CNF and CNC, the detection of some particles by light microscopy suggested that the capsule thickness was higher than in the case of Chit capsules. This was in agreement with the increase in thickness observed during the multilayer growth by QCM-D and ellipsometry. Indeed, the adsorption of xyloglucan resulted in thicker layers than Chit; however, the water uptake was greater in the case of Chit multilayers.

Conclusions

This work demonstrates the possibility of fabricating self-supported systems by taking advantage of the interactions

between polysaccharides. The supramolecular architectures are based on the specific association between cellulose and xyloglucan by hydrogen bonds and van der Waals interactions, and the electrostatic interaction between the negatively charged TEMPO-oxidized cellulose and the positively charged chitosan. Results evidence the impact of the effect of charge on polysaccharide interaction. The highly specific interaction between cellulose and xyloglucan facilitates the supramolecular assembly and the multilayer growth, which imparts the stability when removing the template. The rod-like and rigid nature of CNC also contributes to the hollow capsule stabilization. Concluding, the combination of CNC and XG yields the most stable supramolecular assemblies when template is removed.

Acknowledgments: The authors gratefully acknowledge the Conseil Régional des Pays de la Loire (Project Nanomach, Etoiles Montantes 2017-10691) for financial support. The authors acknowledge the BIBS platform of INRAE Angers-Nantes for the access to CLSM (Bruno Novales).

Funding: This work was funded by the Conseil Régional des Pays de la Loire (Project Nanomach, Etoiles Montantes 2017-10691).

Conflict of interest: The authors declare no conflicts of interest.

References

Ahola, S., Osterberg, M., et al. (2008a) Cellulose nanofibrils-adsorption with poly(amideamine) epichlorohydrin studied by QCM-D and application as a paper strength additive. Cellulose 15(2):303–314.

Ahola, S., Salmi, J., et al. (2008b) Model films from native cellulose nanofibrils. Preparation, swelling, and surface interactions. Biomacromolecules 9(4):1273–1282.

Amirkhani, M., Volden, S., et al. (2008) Adsorption of cellulose derivatives on flat gold surfaces and on spherical gold particles. J. Colloid Interface Sci. 328(1):20–28.

Aulin, C., Johansson, E., et al. (2010) Self-Organized Films from Cellulose I Nanofibrils Using the Layer-by-Layer Technique. Biomacromolecules 11(4):872–882.

Belder, A.N.D., Granath, K. (1973) Preparation and properties of fluorescein-labeled dextrans. Carbohydr. Res. 30(2):375–378.

Charreau, H., Cavallo, E., et al. (2020) Patents involving nanocellulose: Analysis of their evolution since 2010. Carbohydr. Polym. 237.

Cherhal, F., Cousin, F., et al. (2016) Structural Description of the Interface of Pickering Emulsions Stabilized by Cellulose Nanocrystals. Biomacromolecules 17(2):496–502.

Corrêa-Filho, L., Moldão-Martins, M., et al. (2019) Advances in the Application of Microcapsules as Carriers of Functional Compounds for Food Products. Appl. Sci. 9(3):571.

Cranston, E.D., Gray, D.G. (2006) Morphological and optical characterization of polyelectrolyte multilayers incorporating nanocrystalline cellulose. Biomacromolecules 7(9):2522–2530.

de Castro, D.O., Tabary, N., et al. (2018) Controlled release of carvacrol and curcumin: bio-based food packaging by synergism action of TEMPO-oxidized cellulose nanocrystals and cyclodextrin. Cellulose 25(2):1249–1263.

Dias, M.I., Ferreira, I.C., et al. (2015) Microencapsulation of bioactives for food applications. Food Funct. 6(4):1035–1052.

Eichhorn, S.J., Dufresne, A., et al. (2011) Review: current international research into cellulose nanofibres and nanocomposites. J. Mater. Sci. 45(1):1–33.

Eronen, P., Junka, K., et al. (2011) Interaction between water-soluble polysaccharides and native nanofibrillar cellulose thin films. BioResources 6(4):4200–4217.

Habibi, Y., Chanzy, H., et al. (2006) TEMPO-mediated surface oxidation of cellulose whiskers. Cellulose 13(6):679–687.

Hatakeyama, H., Hatakeyama, T. (1998) Interaction between water and hydrophilic polymers. Thermochim. Acta 308(1-2):3–22.

Huq, T., Salmieri, S., et al. (2012) Nanocrystalline cellulose (NCC) reinforced alginate based biodegradable nanocomposite film. Carbohydr. Polym. 90(4):1757–1763.

Jiménez-Saelices, C., Seantier, B., et al. (2017) Spray freeze-dried nanofibrillated cellulose aerogels with thermal superinsulating properties. Carbohydr. Polym. 157:105–113.

Jiménez-Saelices, C., Seantier, B., et al. (2018) Thermal Superinsulating Materials Made from Nanofibrillated Cellulose-Stabilized Pickering Emulsions. ACS Appl. Mater. Interfaces 10(18):16193–16202.

Kalashnikova, I., Bizot, H., et al. (2013) Cellulosic nanorods of various aspect ratios for oil in water Pickering emulsions. Soft Matter 9(3):952–959.

Kittle, J.D., Du, X., et al. (2011) Equilibrium Water Contents of Cellulose Films Determined via Solvent Exchange and Quartz Crystal Microbalance with Dissipation Monitoring. Biomacromolecules 12:2881–2887.

Kittle, J.D., Wang, C., et al. (2012) Ultrathin chitin films for nanocomposites and biosensors. Biomacromolecules 13(3):714–718.

Klemm, D., Cranston, E.D., et al. (2018) Nanocellulose as a natural source for groundbreaking applications in materials science: Today's state. Mater. Today 21(7):720–748.

Lin, N., Huang, J., et al. (2011) Effect of polysaccharide nanocrystals on structure, properties, and drug release kinetics of alginate-based microspheres. Colloids Surf. B, Biointerfaces 85(2):270–279.

Lin, N., Huang, J., et al. (2012) Preparation, properties and applications of polysaccharide nanocrystals in advanced functional nanomaterials: a review. Nanoscale 4(11):3274–3294.

Lombardo, S., Gencer, A., et al. (2019) Thermodynamic Study of Ion-Driven Aggregation of Cellulose Nanocrystals. Biomacromolecules 20(8):3181–3190.

Lombardo, S., Thielemans, W. (2019) Thermodynamics of adsorption on nanocellulose surfaces. Cellulose 26(1):249–279.

Lombardo, S., Villares, A. (2020) Engineered Multilayer Microcapsules Based on Polysaccharides Nanomaterials.

Molecules 25:19.
Martin, C., Bruno, J. (2014) Nanocellulose/polymer multilayered thin films: tunable architectures towards tailored physical properties. Nord. Pulp Pap. Res. J. 29(1):19–30.
Mohanta, V., Madras, G., et al. (2014) Layer-by-Layer Assembled Thin Films and Microcapsules of Nanocrystalline Cellulose for Hydrophobic Drug Delivery. ACS Appl. Mater. Interfaces 6(22):20093–20101.
Moreau, C., Villares, A., et al. (2016) Tuning supramolecular interactions of cellulose nanocrystals to design innovative functional materials. Ind. Crop. Prod. 93:96–107.
Muller, M., Czihak, C., et al. (2000) All disordered regions of native cellulose show common low-frequency dynamics. Macromolecules 33(5):1834–1840.
Niinivaara, E., Faustini, M., et al. (2015) Water Vapor Uptake of Ultrathin Films of Biologically Derived Nanocrystals: Quantitative Assessment with Quartz Crystal Microbalance and Spectroscopic Ellipsometry. Langmuir 31(44):12170–12176.
Olszewska, A.M., Kontturi, E., et al. (2013) All-cellulose multilayers: long nanofibrils assembled with short nanocrystals. Cellulose 20(4):1777–1789.
Paulraj, T., Riazanova, A.V., et al. (2017) Bioinspired Layer-by-Layer Microcapsules Based on Cellulose Nanofibers with Switchable Permeability. Biomacromolecules 18(4):1401–1410.
Paulraj, T., Riazanova, A.V., et al. (2018a) Bioinspired capsules based on nanocellulose, xyloglucan and pectin – The influence of capsule wall composition on permeability properties. Acta Biomater. 69:196–205.
Paulraj, T., Wennmalm, S., et al. (2018b) Porous Cellulose Nanofiber-Based Microcapsules for Biomolecular Sensing. ACS Appl. Mater. Interfaces 10(48):41146–41154.
Paulraj, T., Wennmalm, S., et al. (2020) Primary cell wall inspired micro containers as a step towards a synthetic plant cell. Nat. Commun. 11(1):958.
Rodahl, M., Hook, F., et al. (1997) Simultaneous frequency and dissipation factor QCM measurements of biomolecular adsorption and cell adhesion. Faraday Discuss. 107:229–246.
Sauerbrey, G. (1959) Verwendung von Schwingquarzen zur Wägung dünner Schichten und zur Mikrowägung. Z. Phys. 155(2):206–222.
Villares, A., Moreau, C., et al. (2014) Impact of Ionic Strength on Chitin Nanocrystal-Xyloglucan Multilayer Film Growth. Biopolymers 101(9):924–930.
Wagberg, L., Decher, G., et al. (2008) The build-up of polyelectrolyte multilayers of microfibrillated cellulose and cationic polyelectrolytes. Langmuir 24(3):784–795.
Wagberg, L., Erlandsson, J. (2020) The Use of Layer-by-Layer Self-Assembly and Nanocellulose to Prepare Advanced Functional Materials. Adv. Mater. 2001474.
Zhang, Q., Brumer, H., et al. (2011) The adsorption of xyloglucan on cellulose: effects of explicit water and side chain variation. Carbohydr. Res. 346(16):2595–2602.

Supplemental Material: The online version of this article offers supplementary material (https://doi.org/10.1515/npprj-2021-0040).